Research Article

Zhaohui Wang, Yang Liao*, Peng Wang, Jia Qi, Lingling Qiao, Koji Sugioka and Ya Cheng*

Formation of in-volume nanogratings in glass induced by spatiotemporally focused femtosecond laser pulses

DOI 10.1515/aot-2015-0058
Received December 1, 2015; accepted December 27, 2015; previously published online February 3, 2016

Abstract: We present comparative investigations on the formation of in-volume nanogratings in a porous glass with both conventionally and spatiotemporally focused femtosecond laser pulses. Our results show that despite the different spatiotemporal characteristics of the light fields produced at the foci with the two focusing schemes, nanogratings can be formed in both cases, whereas their structural features are different. We discuss the physical mechanism behind the experimental observations.

Keywords: nanograting; porous glass; spatiotemporal focusing.

***Corresponding authors: Yang Liao and Ya Cheng,** State Key Laboratory of High Field Laser Physics, Shanghai Institute of Optics and Fine Mechanics, Chinese Academy of Sciences, Shanghai 201800, China, e-mail: superliao@vip.sina.com (Y. Liao), ya.cheng@siom.ac.cn (Y. Cheng)
Zhaohui Wang: State Key Laboratory of High Field Laser Physics, Shanghai Institute of Optics and Fine Mechanics, Chinese Academy of Sciences, Shanghai 201800, China; and University of Chinese Academy of Sciences, Beijing 100049, China
Peng Wang and Jia Qi: State Key Laboratory of High Field Laser Physics, Shanghai Institute of Optics and Fine Mechanics, Chinese Academy of Sciences, Shanghai 201800, China; and School of Physical Science and Technology, ShanghaiTech University, Shanghai 200031, China
Lingling Qiao: State Key Laboratory of High Field Laser Physics, Shanghai Institute of Optics and Fine Mechanics, Chinese Academy of Sciences, Shanghai 201800, China
Koji Sugioka: RIKEN-SIOM Joint Research Unit, RIKEN Center for Advanced Photonics, 2-1 Hirosawa, Wako, Saitama 351-0198, Japan

1 Introduction

Femtosecond laser micromachining has emerged to become one of the most promising applications of ultrafast laser technology because it provides many unique advantages, including high spatial resolution, three-dimensional fabrication capacity, versatility of materials that can be processed, and flexibility of multifunctional integration [1–6]. Recently, interaction of spatiotemporally focused (STF) femtosecond laser pulses with transparent materials has attracted much attention due to the unconventional spatiotemporal characteristics such as a varying pulse width during propagation [7], a tilted pulse front [8, 9], and a tilted peak intensity distribution [10]. The working principle of the technique is to first spatially chirp the incident pulse before the focal lens, forming an array of beamlets at different frequencies. This leads to the elongation of the pulse duration due to the reduction of the bandwidth of each beamlet. After passing through the focal lens, all of the beamlets will be recombined at the focal plane, where the original broadband spectrum of the incident femtosecond pulse is restored to give rise to the shortest pulses. Before or after the focal plane, the beamlets only partially overlap, leading to stretched pulse durations as a result of the reduced bandwidth as well as a pulse chirping. In such a manner, the peak intensity of the STF pulses is strongly localized near the geometrical focus, so that the longitudinal resolution is improved in the interaction of the STF pulses with transparent materials.

On the other hand, formation of self-organized nanogratings in bulk glasses with femtosecond laser pulses is one of the current most intriguing phenomena in the interactions of light with transparent materials [11–13]. With the feature sizes far beyond the optical diffraction limit, these nanostructures have found widespread applications in nanophotonics and nanofluidics [14–16]. Recently, we accessed the snapshots of morphologies in the laser-affected regions in a porous glass, which reveal the evolution of the formation of nanogratings with

increasing number of laser pulses [17, 18]. We observed that surface plasma waves excited at the interface played an important role in the formation of nanogratings, which shed light on the mechanism behind nanostructuring in transparent materials. Based on such consideration, it is logical to examine the evolution of the formation of nanogratings in glass with STF pulses, as these pulses provide versatile control parameters for tuning the properties of the plasma waves with enhanced flexibility. In this paper, we present comparative investigations on the formation of in-volume nanogratings in a porous glass with both conventionally focused (CF) and STF femtosecond laser pulses. The finding will further deepen the understanding of the physical mechanism behind the nanograting formation and benefit the control of geometries of the nanogratings with the shaped laser pulses.

2 Experiment

Figure 1 schematically illustrates the experimental setup. In our experiment, high-silicate porous glass samples were used as the substrates, which were produced by removing the borate phase from phase-separated alkali-borosilicate glass in a hot acid solution [19]. Details of the glass can be found elsewhere [20]. To induce the nanograting structures, a high-repetition regeneratively amplified Ti:sapphire laser (Coherent Inc., RegA 9000, Santa Clara, CA, USA), which delivers ~100 fs, *p*-polarized pulses centered at 800-nm wavelength at a 250-kHz repetition rate, was employed. The laser beam had a beam diameter of ~8.8 mm. In the STF scheme as shown in Figure 1A, a pair of parallel gratings (300 lines/mm; Thorlabs Inc., Newton, NJ, USA) was used to separate the spectral components of the incident beam along the x-axis. The distance between the gratings was set to be ~200 mm, and the incident angle was

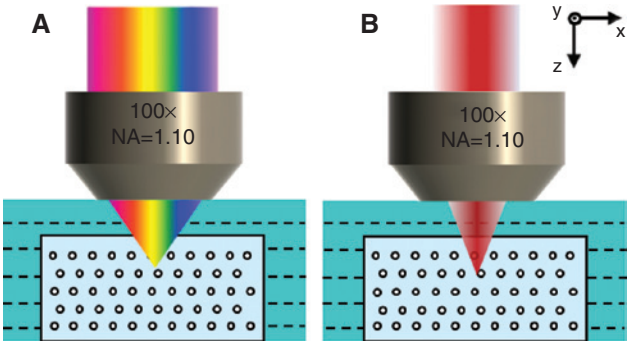

Figure 1: Schematic illustrations of femtosecond laser direct writing setups with (A) a spatiotemporally focused beam and (B) a conventionally focused beam.

0° (i.e. the input beam perpendicularly incident upon the grating). A variable neutral density filter and an adjustable circular aperture were inserted in series before the gratings to adjust the power and the initial size of the input beam. In the STF scheme, the input laser beam size was set to be ~3 mm. After being dispersed by the grating pair, the laser beam was measured to be ~6 mm ($1/e^2$) along the x-axis and ~3 mm ($1/e^2$) along the y-axis. To precompensate the chirp induced by the grating pair, the input pulse was positively prechirped by adjusting the compressor in the amplifier. It should be noted that during the experiment, the polarization direction of the laser beam was set along the x-axis, which was parallel to the spatial chirp. This is because the essential properties of the STF ultrafast pulses are the pulse front tilting (PFT) and intensity plane tilting (IPT). The PFT indicates that the focused pulse does not arrive at the focal plane at the same time; instead, the peak intensity will sweep across the focal plane along the direction of the spatial chirp. The IPT indicates that the peak intensity of STF pulses does not distribute exactly at the focal plane. As a result, the focal spot will appear tilted in the plane parallel to the direction of spatial chirp of the incident pulse but perpendicular to the optical axis. Both these interesting effects of STF pulses can only be observed in the direction parallel to direction of the spatial chirp. To observe how these two effects influence the nanograting formation, the nanoplanes in the nanogratings must be perpendicular to the direction of the spatial chirp. Such nanogratings can only be generated when the polarization direction of the laser beam is parallel to the direction of the spatial chirp, which leads to the coupling of the effects of STF pulses into the nanograting formation. Meanwhile, the writing direction was along the y-axis. In contrast, the CF scheme (Figure 1B) was simply achieved by replacing the grating pair with a pair of flat gold mirrors. An autocorrelator was utilized to optimize the pulse width and minimize the spatiotemporal distortions of the beam when the CF scheme was employed. The input beam size was first set to be ~3 mm (same as the input beam size of the STF scheme) and then changed to ~8 mm (the full aperture of the objective lens) in the experiments using the CF scheme.

A long-working-distance water-immersion objective lens [numerical aperture (NA)=1.10] (Olympus Inc., Takeshi, Tokyo, Japan) was employed for focusing the beam into porous glass at a depth of ~170 μm below the surface. The glass sample was fixed in a Petri dish filled with distilled water. It is worth mentioning that as the water immersion objective was used in the experiment, spherical aberration was practically eliminated in the focusing geometries. To characterize the morphologies of the embedded nanogratings, the fabricated samples were

cleaved without further polish along the plane perpendicular to the writing direction to access the cross sections of the laser-modified zones. The revealed nanograting structures were directly characterized using a scanning electron microscope (SEM; Zeiss Auriga 40, Carl Zeiss AG, Oberkochen, Germany).

3 Experimental results

First, we present SEM images of the cross sections of nanograting inscribed in porous glass induced by STF and CF pulses. The pulse energy was ~68 nJ, which is slightly above the ablation threshold. The scan velocity was set to be 200 μm/s. In such experimental conditions, periodic nanogratings were formed with a height of ~1.6 μm and a transverse period of ~200 nm by the STF as shown in Figure 2A. It can be observed that the distribution of the nanoplanes in the nanograting shows an asymmetrical profile, i.e. the nanoplanes on the right-hand side are lower than that on the left-hand side. When the grating pair was replaced by a pair of flat gold mirrors, i.e. the spatial chirp of the beam was removed, whereas all the other conditions were unchanged, the nanograting induced by the CF beam is shown in Figure 2B. We notice that the heights of the nanoplanes in the nanograting are longer than that of the nanogratings in Figure 2A, as the STF can significantly improve the depth of focus [7]. However, the grating period remains to be ~200 nm. The nanograting induced by the CF scheme with a full-size beam (~8 mm) is presented in Figure 2C. The pulse energy was reduced to be ~37 nJ due to the tighter focusing, and the scan velocity was kept to be 200 μm/s. As shown in Figure 2C, the height of the nanograting is reduced as compared to both the nanogratings in Figure 2A and B due to the tighter focusing condition (i.e. the NA is increased as a result of the large diameter of the incident beam). As we have discussed in detail in Ref. [21], once the back aperture of an objective lens is completely filled, the CF scheme always leads to the strongest axial intensity localization in comparison with the STF scheme, as the diameter of the incident beam must be significantly reduced in the STF to allow for a spatial chirp at the back aperture of the objective lens. By making comparisons among the results in Figure 2, we find that the asymmetrical distribution of the nanograting can only be observed in the STF scheme.

To gain a deep insight of the phenomenon observed in Figure 2, we attempt to visualize the formation of the nanogratings using different focusing schemes. The SEM images of the cross sections of the nanostructures induced by the STF beam at a pulse energy of 68 nJ and various scan velocities are shown in Figure 3. At the highest scan velocity of 4000 μm/s, which corresponds to the least number of laser pulses deposited in the focal volume, a well-defined laser-modified zone can be formed in which a large number defects are formed as shown in Figure 3A. In essence, the defects are nanovoids with sizes significantly larger than the original pores in the porous glass, which are formed by microexplosions induced in the porous glass by femtosecond laser irradiation. Interestingly, the laser-modified zone is obviously tilted with respect to the direction of laser propagation, and the tilt angle is measured to be ~20°, as indicated by the red dashed lines. With an increasing number of pulses, some signature of periodically arranged nanovoid array appears in the tilted laser-modified zone, as shown in Figure 3B. After irradiation with sufficient number of laser pulses, the nanovoid array grows into subwavelength-width nanoplanes, as shown in Figure 3C. In addition, the nanograting appears asymmetric, as the distribution of the initial defects formed by the first few pulses has an asymmetric profile. Further reduction of the scan velocity leads to the extension of the grating length along the propagation direction; however, the key features such as the period and the asymmetrical distribution remain unchanged, as shown in Figure 3D,E. The evolution of the formation of nanogratings induced by the STF pulses indicates that the final asymmetric profile of the nanograting can be attributed to the asymmetric distribution of the initial defects irradiated by the first a few pulses. In contrast, when the CF scheme was used, the evolution of the formation of nanogratings is presented in Figure 4. It is obvious that in Figure 4A–E, the profiles of the laser-affected zones are always symmetric. The evolution process of the formation of nanogratings is similar to the results as we have reported in Ref. [11]. We will discuss the likely physical mechanism behind the phenomenon.

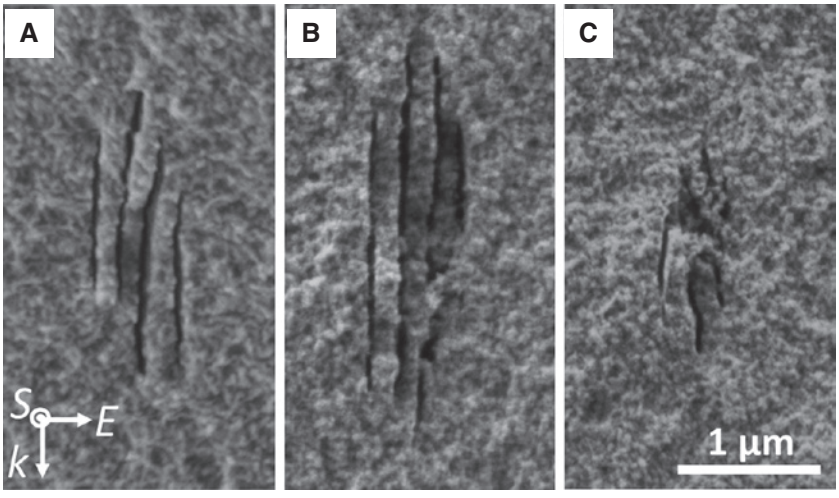

Figure 2: Cross-sectional morphologies of nanogratings written with (A) spatiotemporally focused beam, (B) conventionally focused beam with a reduced diameter, and (C) conventionally focused beam with a full-size beam. The laser incident direction (*k*), polarization direction (*E*), and the writing direction (*S*) are indicated in the figure.

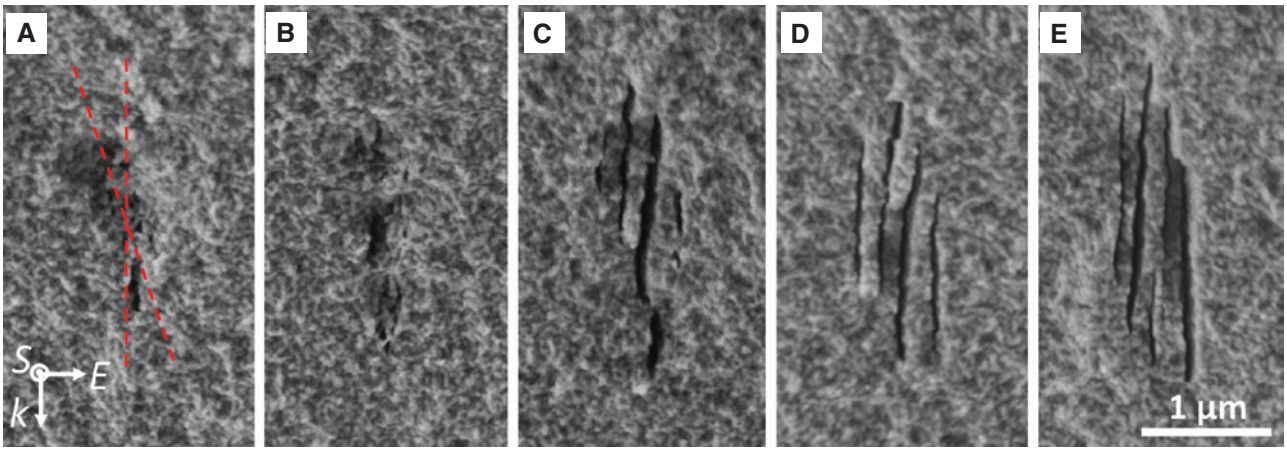

Figure 3: Cross-sectional morphologies of nanogratings written with spatiotemporally focused beam. The scan velocities in (A) to (E) are 4000, 3000, 750, 200, and 30 μm/s, respectively. The laser incident direction (*k*), polarization direction (*E*), and the writing direction (*S*) are indicated in the figure.

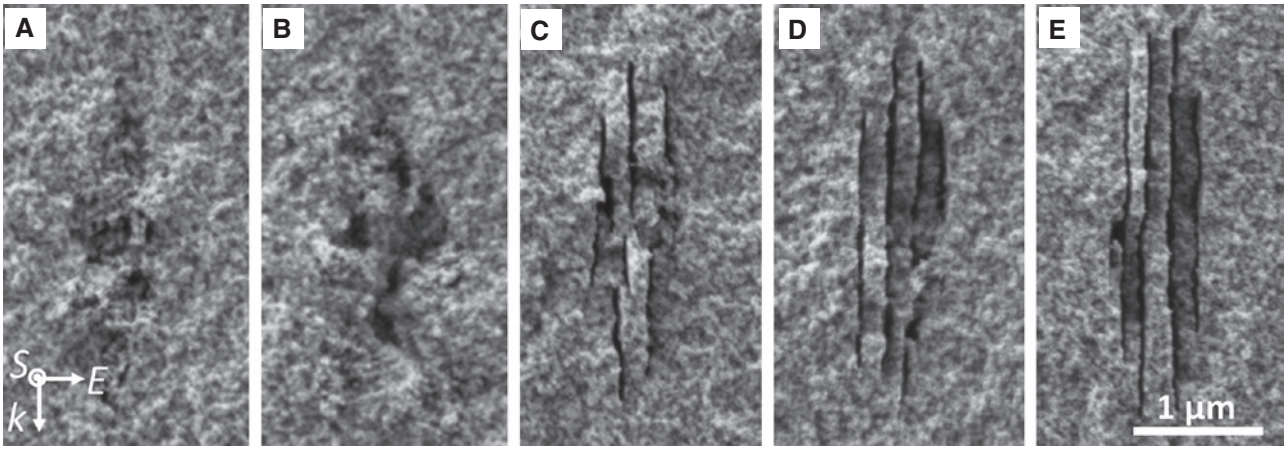

Figure 4: Cross-sectional morphologies of nanogratings written with conventionally focused beam with a reduced diameter. The scan velocities in (A) to (E) are 4000, 3000, 750, 200, and 30 μm/s, respectively. The laser incident direction (*k*), polarization direction (*E*), and the writing direction (*S*) are indicated in the figure.

4 Discussion

The asymmetric distribution of the initial defects induced by the STF laser pulses can be attributed to the IPT of the focal spot [10], as evidenced by our theoretical analysis below. The normalized light field of a spatially dispersed pulse E_1 at the entrance aperture of the objective lens can be expressed as [7]

$$E_1(x, y, \omega)=E_0 \exp\left[-\frac{(\omega-\omega_0)^2}{\Delta\omega^2}\right]\exp\left\{-\frac{\left[x-\alpha(\omega-\omega_0)\right]^2+y^2}{w_{in}^2}\right\}, \quad (1)$$

where E_0 is the constant field amplitude, ω_0 the carrier frequency, $\Delta\omega$ the bandwidth ($1/e^2$ half width) of the pulses, and w_{in} the initial beam waist ($1/e^2$). $\alpha(\omega-\omega_0)$ is the linear shift of each spectral component of the spatially dispersed pulse. The laser field near the focal spot can be obtained using the Fresnel diffraction formula:

$$E_2(x, y, z, \omega)=\frac{\exp(ikz)}{i\lambda z}\int\int_{-\infty}^{\infty} E_1(\xi, \eta, \omega)\exp\left(-ik\frac{\xi^2+\eta^2}{2f}\right)\exp\left(ik\frac{(x-\xi)^2+(y-\eta)^2}{2z}\right)d\xi d\eta. \quad (2)$$

For our experimental conditions (α=2.1×10^{-17} m/rad, w_{in}=1.5 mm, $\Delta\omega$=1.1×10^{14} s^{-1}), the aperture of the objective lens was not fully filled with the spatial-chirped beam, leading to the reduction of the NA. Considering that the refractive index of the porous glass immersed in water

is ~1.40 based on the volume ratio of pores ~40%, and the aperture of the objective lens is not fully filled by the spatial chirped beam, an NA of 0.86 was chosen in our simulation based on the experimental parameters. The intensity distribution in the time domain can be calculated by

$$I(x, y, z, t)=\left|E_3(x, y, z, t)\right|^2=\left|\mathcal{F}^{-1}\left[E_2(x, y, z, \omega)\right]\right|^2. \quad (3)$$

The calculated intensity distribution of the focal spot in the XZ plane is shown in Figure 5. One can see that the peak intensity distribution is asymmetric and tilted by ~20° with respect to the z-axis, as indicated by the black dashed lines. The calculated tilting angle as indicated in Figure 5 agrees well with the tilting angle of the laser-affected zone in Figure 3A, indicating that, indeed, the asymmetric distributions of the nanogratings originate from the IPT effect of the STF pulses.

5 Conclusion

To conclude, we have examined the evolutions of nanograting formation in porous glass with both the CF and STF irradiation pulses. We observed that in the case of using the STF scheme, the nanoplanes in the nanogratings are asymmetrically distributed, which originates from a tilted interface initially produced in glass by the STF pulses. The tilted interface can be attributed to the IPT, which was first observed by He et al. in 2014 [10].

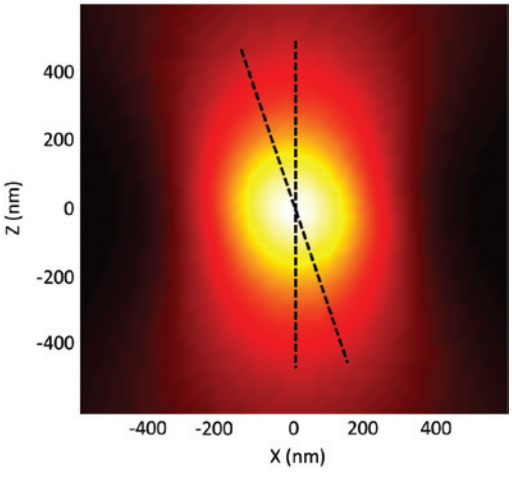

Figure 5: Numerically calculated laser intensity distribution at the focus with STF scheme in the XZ plane.

Our results also show that the nanogratings produced by the STF pulses are shorter in their height (along the axial direction) than that produced by the CF scheme. The higher axial resolution will benefit applications such as nanooptics and nanofluidics.

Acknowledgments: This work was supported by the National Basic Research Program of China (grant no. 2014CB921300) and National Natural Science Foundation of China (grant nos. 61327902, 11134010, 61275205, and 11304330).

References

[1] R. R. Gattass and E. Mazur, Nat. Photon. 2, 219–225 (2008).
[2] K. Sugioka and Y. Cheng, Light Sci. Appl. 3, e149 (2014).
[3] R. Osellame, H. J. Hoekstra, G. Cerullo and M. Pollnau, Laser Photon. Rev. 5, 442–463 (2011).
[4] M. Beresna, M. Gecevičius, and P. G. Kazansky, Adv. Opt. Photon. 6, 293–339 (2014).
[5] M. Ams, G. D. Marshall, P. Dekker, J. A. Piper and M. J. Withford, Laser Photon. Rev. 3, 535–544 (2009).
[6] F. Chen and J. R. Aldana, Laser Photon. Rev. 8, 251–275 (2014).
[7] F. He, H. Xu, Y. Cheng, J. Ni, H. Xiong, et al., Opt. Lett. 35, 1106 (2010).
[8] D. N. Vitek, E. Block, Y. Bellouard, D. E. Adams, S. Backus, et al., Opt. Express 18, 24673–24678 (2010).
[9] Z. Wang, F. He, J. Ni, C. Jing, H. Xie, et al., Opt. Express 22, 26328–26337 (2014).
[10] F. He, B. Zeng, W. Chu, J. Ni, K. Sugioka, et al., Opt. Express 22, 9734–9748 (2014).
[11] P. G. Kazansky, H. Inouye, T. Mitsuyu, K. Miura, J. Qiu, et al., Phys. Rev. Lett. 82, 2199–2202 (1999).
[12] Y. Shimotsuma, P. G. Kazansky, J. Qiu and K. Hirao, Phys. Rev. Lett. 91, 247405 (2003).
[13] V. R. Bhardwaj, E. Simova, P. P. Rajeev, C. Hnatovsky, R. S. Taylor, et al., Phys. Rev. Lett. 96, 057404 (2006).
[14] Y. Shimotsuma, M. Sakakura, P. G. Kazansky, M. Beresna, J. Qiu, et al., Adv. Mater. 22, 4039–4043 (2010).
[15] M. Beresna, M. Gecevicius, P. G. Kazansky and T. Gertus, Appl. Phys. Lett. 98, 201101 (2011).
[16] Y. Liao, Y. Cheng, C. Liu, J. Song, F. He, et al., Lab Chip 13, 1626–1631 (2013).
[17] Y. Liao, J. Ni, L. Qiao, M. Huang, Y. Bellouard, et al., Optica 2, 329–334 (2015).
[18] Y. Liao, W. Pan, Y. Cui, L. Qiao, Y. Bellouard, et al., Opt. Lett. 40, 3623–3626 (2015).
[19] T. H. Elmer, Porous and Reconstructed Glasses, Vol. 4 of Engineered Materials Handbook (ASM International, 1992), pp. 427–432.
[20] Y. Liao, Y. Shen, L. Qiao, D. Chen, Y. Cheng, et al., Opt. Lett. 38, 187–189 (2013).
[21] Y. Cheng, H. Xie, Z. Wang, G. Li, B. Zeng, et al., Phys. Rev. A 92, 023854 (2015).